DSN In-Band Continuous-Wave Radio Frequency Interference-Suppression Techniques

H. Tsou[1] and M. Srinivasan[1]

Radio frequency interference has been a potential threat to the operation of NASA's Deep Space Network. Despite regulatory efforts to avoid potential sources of such interference, the increasing crowding of the S-band (2.3-GHz) and X-band (8.4-GHz) spectra inevitably limits the effectiveness of frequency management efforts. In this article, two interference-suppression schemes for in-band continuous-wave interferences using either the time-domain adaptive filtering technique or the frequency-domain filtering technique are presented. The simulated performances based upon the tracking of a fully suppressed binary phase-shift keyed signal are compared, and trade-offs between them are discussed. The results show the time-domain approach to be the best method to mitigate the in-band continuous-wave type of radio frequency interference, while the frequency-domain approach potentially can deal with out-of-band interferences.

I. Introduction

With supersensitive radio frequency front ends, the Deep Space Network (DSN) receivers are highly susceptible to radio frequency interference (RFI). RFI has been a continuous threat to the operation of the DSN, especially in recent times as the frequency spectrum has become congested with many new NASA missions. There also are potential threats from emerging wireless services.[2] RFI within DSN complexes also has been reported. For example, the Goldstone solar system radar at DSS 14 interferes with downlink reception at the nearby DSS 15. Furthermore, an induced-burst type of broadband interference also has been observed during tracking operation of the 70-m antenna at Goldstone. This RFI problem is alleged to be from the imperfection of the surface condition and the structure alteration to the antenna and may become a problem during a spacecraft emergency when both high transmitting power and high receiver sensitivity are required.[3] Although many potential RFI problems can be avoided by careful spectrum management and active coordination, it has become evident that RFI-mitigation techniques will be needed in the future.

Depending on the affected frequency spectrum, the RFI can be classified as in-band or out-of-band. The in-band RFI, which affects the main portion of the spectrum occupied by a DSN telemetry signal, can cause problems such as false lock, drop of lock, etc., to the receiver, rendering severe performance

[1] Communications Systems and Research Section.

[2] P. Robbins, *Preliminary DSN RFI Study, Deep Space—Space Research Bands*, JPL Interoffice Memorandum 3396-94-01 (internal document), Jet Propulsion Laboratory, Pasadena, California, January 19, 1994.

[3] A. Freiley, personal communication, Jet Propulsion Laboratory, Pasadena, California, December 1996.

degradation. The out-of-band RFI, which is not covered by the receiver's bandwidth but is still inside the much wider bandwidth of the RF front end, such as the maser or high electron-mobility transistor (HEMT) low-noise amplifier (LNA), can cause a gain saturation problem in the LNA and effectively reduce the available signal-to-noise ratio (SNR) in the subsequent signal processing.

In this article, we will focus on the in-band RFI and provide mitigation techniques from the signal-processing point of view for solving the problem caused by in-band continuous-wave (CW) RFI. In Section II, CW RFI suppression using the adaptive line enhancer (ALE) will be discussed. This is a time-domain approach using an adaptive algorithm to "learn" the RFI characteristics and eventually cancel the RFI. A frequency-domain approach facilitated by real-time, high-resolution, discrete-Fourier-transform (DFT) equipment known as the channelized signal processor (CSP) is discussed in Section III. The bit-error performances of these two RFI-suppression techniques are simulated to demonstrate the effectiveness of these approaches. These results are presented and compared in Section IV, followed by the conclusion in Section V.

II. Time-Domain Adaptive CW RFI Suppression

The ALE was first introduced by Widrow et al. [1] as a least-mean-square (LMS) adaptive filtering technique to separate the periodic component from the broadband components of the input signal. The initial application of the ALE primarily was for detecting the presence of sinusoid(s) in white noise, such as in fast carrier acquisition. However, because of its nature of exploring the difference between the correlation times of the signal and noise, the ALE has been found useful for many other applications [2–4], such as spectral analysis, speech encoding, narrowband interference rejection, etc.

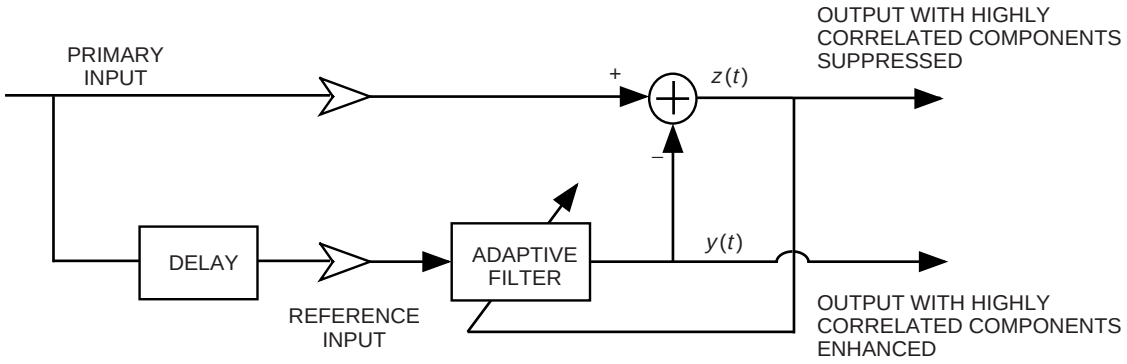

Fig. 1. The time-domain CW RFI-suppression scheme.

As shown in Fig. 1, the ALE consists of two channels: the primary channel and the reference channel. The primary and reference channels share the same input signal. However, the latter contains a fixed delay that functions as a decorrelator to the broadband noise components existing in both channels. The delayed version of the input signal in the reference channel is adaptively filtered and then subtracted from the real-time input signal in the primary channel to form a difference signal that serves as the error signal for the LMS algorithm. The LMS algorithm controls the weights of the adaptive filter in such a way that the power of the difference signal is minimized. Operation of the ALE can be illustrated simply as follows: Mathematically, the error signal to be minimized in the mean-square sense is modeled by

$$z(t_k) = [s(t_k) + n(t_k)] - [\tilde{s}(t_k) + \tilde{n}(t_k)] \tag{1}$$

where $s(t_k)$ is a narrowband signal component, $n(t_k)$ is the statistically independent broadband noise component received in the primary channel, and $\tilde{s}(t_k)$ and $\tilde{n}(t_k)$ are the filtered signal and noise components, given as follows:

$$\tilde{s}(t_k) = \sum_{i=0}^{N-1} w_{k-i}(t_k) s(t_{k-i} - \Delta) \tag{2}$$

and

$$\tilde{n}(t_k) = \sum_{i=0}^{N-1} w_{k-i}(t_k) n(t_{k-i} - \Delta) \tag{3}$$

where $w_i(t_k)$ is the ith weight of the N-stage LMS adaptive algorithm at time t_k, and Δ is the delay introduced to the reference channel. The delay, Δ, is chosen to be long enough so that the broadband noise components, $n(t_k)$ and $\tilde{n}(t_k)$, become uncorrelated and, on the other hand, to be short enough so that the narrowband components, $s(t_k)$ and $\tilde{s}(t_k)$, are still highly correlated. As a result, minimizing the power of the error signal becomes equivalent to the following:

$$\min \; E\left\{z^2(t_k)\right\} = \min \; \left\{E\left\{[s(t_k) - \tilde{s}(t_k)]^2\right\} + E\{\tilde{n}^2(t_k)\}\right\} \tag{4}$$

Ideally, the LMS algorithm will converge as the weights of the adaptive filter make

$$\left.\begin{array}{l} \tilde{s}(t_k) \;\longrightarrow s(t_k) \\ \\ \tilde{n}(t_k) \;\longrightarrow 0 \end{array}\right\} \tag{5}$$

jointly. Equivalently, the adaptive filter output, $y(t_k)$, and the error signal, $z(t_k)$, will become

$$\left.\begin{array}{l} y(t_k) \;\longrightarrow s(t_k) \\ \\ z(t_k) \;\longrightarrow n(t_k) \end{array}\right\} \tag{6}$$

when the adaptation approaches the steady state. As a result, the ALE effectively separates the highly correlated narrowband signal component from the broadband noise, providing an output with either the signal component suppressed or enhanced depending upon the applications. For carrier acquisition, the residual carrier component can be enhanced so that a better reception is achievable. On the other hand, a CW tone interference can be isolated from the broadband signal for RFI suppression.

The performance of the ALE has been addressed in great detail in many studies [5–10] and will not be repeated here. However, it is important to note the two primary advantages associated with this time-domain adaptive RFI-suppression approach. First, there is no prior knowledge of CW RFI characteristics required when using the ALE. The adaptive algorithm will automatically search for the best combination of filter weights to maximize the separation. Second, it can be incorporated easily into the existing receiver structure as a preprocessor in front of the demodulator without an additional supporting algorithm or hardware device.

III. Frequency-Domain CW RFI Suppression

The narrowband RFI, especially the CW type, also can be rejected by using an adaptive notch filtering technique. It is easier to implement an adaptive notch filter, which is required to have a precise notch

location and sharp cut-off such as an ideal brick-wall filter, on the frequency domain than on the time domain. For example, the narrowband interference can be effectively removed by multiplying the DFT of the input signal segment with a filter mask covering only the affected spectrum. Although it sounds straightforward, this approach involves frequency-domain transformation at the receiver front end, and its success is dependent upon several factors, the most important of which is the very fast, high-resolution DFT that can handle real-time transform processing. The recently deployed CSP at the DSS 14, with its 80-MHz-wide, 2^{22}-channel real-time polyphase-fast-Fourier-transform spectrum analysis capability, is the only equipment qualified for this process.[4]

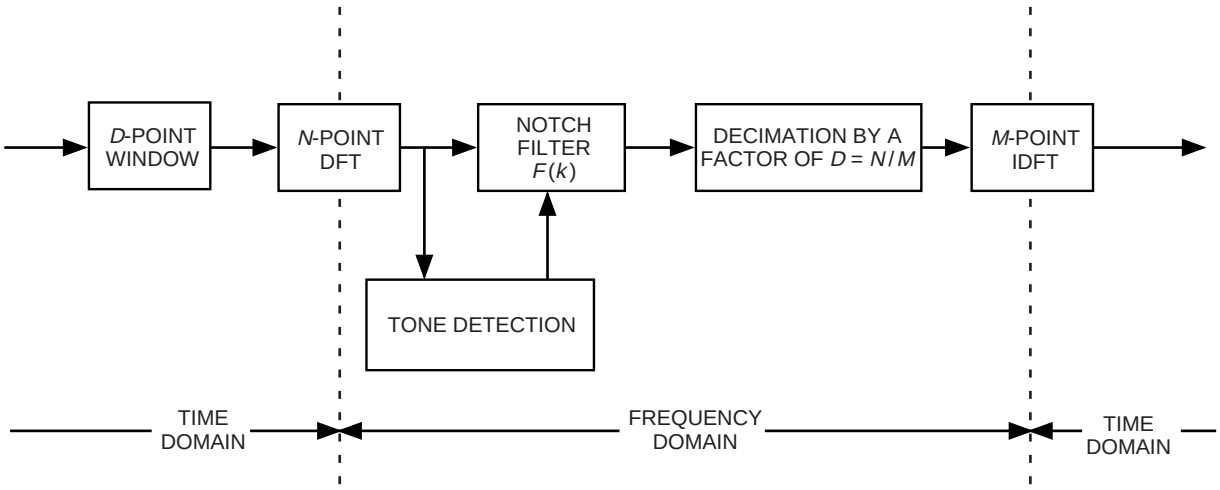

Fig. 2. The frequency-domain CW RFI-suppression scheme.

The transform-domain RFI suppression, as shown in Fig. 2, can be described mathematically as follows: The input signal samples, $x(n)$, are arranged into N-point segments and circularly convolved with a properly chosen D-point window function, $w(n)$, resulting in an N-point windowed input signal, $y(n)$, such that

$$y(n) = \frac{1}{D}\sum_{l=1}^{D} w(l)x(n-l) \tag{7}$$

for $1 \le n \le N$. The N-point DFT of $y(n)$ becomes

$$Y(k) = \sum_{n=1}^{N} y(n)e^{-i2\pi kn/N}$$

$$= \frac{1}{D}\sum_{l=1}^{D} w(l)\sum_{n=1}^{N} x(n-l)e^{-i2\pi kn/N} \tag{8}$$

for $1 \le k \le N$. A desired N-point spectrum mask, $F(k)$, can be applied to this N-point DFT realization so that some elements in $Y(k)$ can be modified. For a CW-type tone interference at frequency f_i, the spectrum mask can be simply chosen as a notch filter:

[4] This equipment is one of the eight filter banks originally designed for the cancelled Search for Extraterrestrial Intelligence (SETI) Sky Survey Project [11].

$$F(k) = \begin{cases} 0, & \left| k - N\left(\frac{f_i}{f_s}\right) \right| \le W_n \\ 1, & \text{otherwise} \end{cases} \tag{9}$$

where f_s is the sampling frequency and W_n is the one-side width in terms of the number of channels (or bins) away from the central channel at $N(f_i/f_s)$. The notch filter then is multiplied with $Y(k)$, effectively nulling out any contribution within the notch, unfortunately including the desired signal. It is important to note that the notch-filter width should be chosen to be large enough to accommodate the first few side lobes of the smeared tone interference, which inevitably is caused by segmenting the input signal samples. The number of side lobes needing to be masked depends upon the relative strength of the interference. For a very strong interference, the side lobes still can have significant impact on the desired signal even though they are far away from the main lobe. After the spectrum mask is applied, the resulting signal needs to be transformed back to the time domain through an inverse DFT (IDFT) for the subsequent receiver functions, which all are performed in the time domain.

Depending upon the processing speed available for the inverse DFT,[5] the masked output may need to be decimated. By forming the decimated M-point signal, $Z(k)$, as follows,

$$Z(k) = \frac{1}{D} \sum_{j=1}^{D} \tilde{Y}[k + (j-1)M] \tag{10}$$

for $1 \le k \le M$, where $M = N/D$ and $\tilde{Y}$ denotes the masked DFT output, the M-point inverse DFT output becomes

$$\hat{y}(n) = \frac{1}{M} \sum_{k=1}^{M} Z(k) e^{i2\pi kn/M} \tag{11}$$

for $1 \le n \le M$. The validity of the decimated inverse DFT can be verified easily, and it is provided in the Appendix.

Although the above operation of narrowband RFI suppression is straightforward , the actual implementation will require additional algorithms to estimate the characteristics of the RFI, especially when the RFI is nonstationary. For example, the location of the tone interference is one of the key parameters to be estimated. This requires a fast detection algorithm and probably a database of possible interference sources to quickly confirm the presence of interference. The relative strength of the interference is another parameter that determines how many side lobes have to be nulled out. Additionally, since the spectrum mask inevitably removes part of the desired signal, some kind of intelligence has to be incorporated into the RFI-detection process to automate the activating and deactivating of the appropriate spectrum mask. This is essential in order to reduce any unnecessary signal loss and improve efficiency by cutting down human intervention. Besides these additional required intelligent detection/estimation algorithms, relying on a single dedicated CSP to facilitate the whole process apparently is a reliability issue to be considered.

IV. Performance Comparison

Both time-domain and frequency-domain RFI-suppression techniques were simulated for their bit-error performances. In these simulations, the desired signal was an uncoded binary phase-shift keyed (BPSK)

[5] Currently, there is no additional dedicated hardware especially designed to provide the vast computing capacity comparable to the CSP. Therefore, it is likely that the inverse DFT can be performed only on a general purpose DSP board, which can handle only a scaled-down computational load as compared with the specialized CSP.

signal with fully suppressed carrier, and the RFI was a fixed-tone interference with various locations and relative strengths. The second-order Costas loop with a loop bandwidth of 0.05 Hz was used for carrier tracking. This setting provided an approximate 33-dB loop signal-to-noise ratio (SNR) when the symbol SNR was at 10 dB. No impact on the symbol-timing synchronization was factored into the simulation results. Figure 3 shows the bit-error performance of the time-domain adaptive approach as a function of the location of the tone interference. The frequencies indicated were normalized to the symbol rate of the uncoded BPSK signal. Therefore, as indicated in the figure, the main lobe of the BPSK signal extended from −1.0 to 1.0, and the tone interference was assumed to be fixed at various positions from the center of the BPSK main lobe (i.e., 0.0) to the center of the BPSK signal's first side lobe (i.e., ±1.5). Different interference-to-signal power ratios, denoted by $J/S = 10$ or 1, also were considered. As expected, the bit-error performance gets worse either when interference becomes stronger or when the interference moves closer to the center of the BPSK main lobe or the first side lobe. Also, larger numbers of LMS weights provide better adaptation, which in turn gives better bit-error performance, as expected. Figure 4 shows the bit-error performance of the time-domain adaptive approach versus the BPSK symbol SNR for different J/S ratios when the tone interference is located halfway between the center of the BPSK main lobe and its first null.

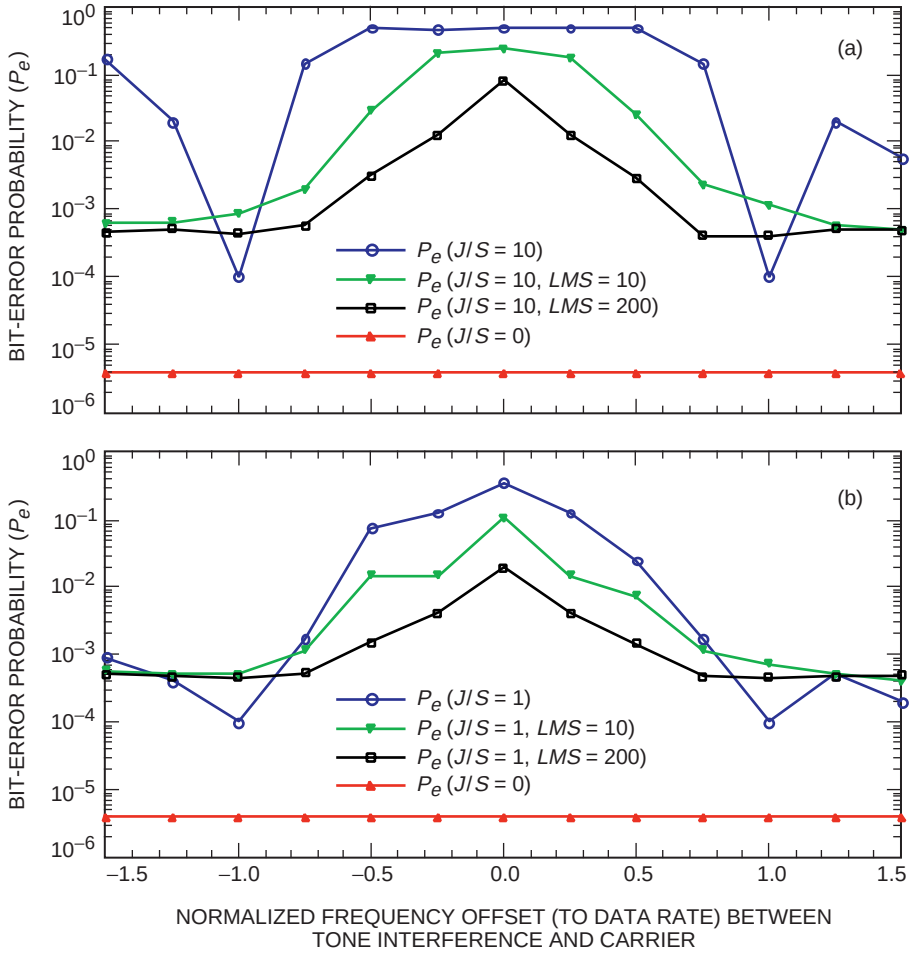

Fig. 3. The bit-error performance of the time-domain RFI-suppression approach as a function of tone interference location, where Δ = 5 bits and *LMS* = the number of taps, when (a) *J*/*S* = 10 and (b) *J*/*S* = 1.

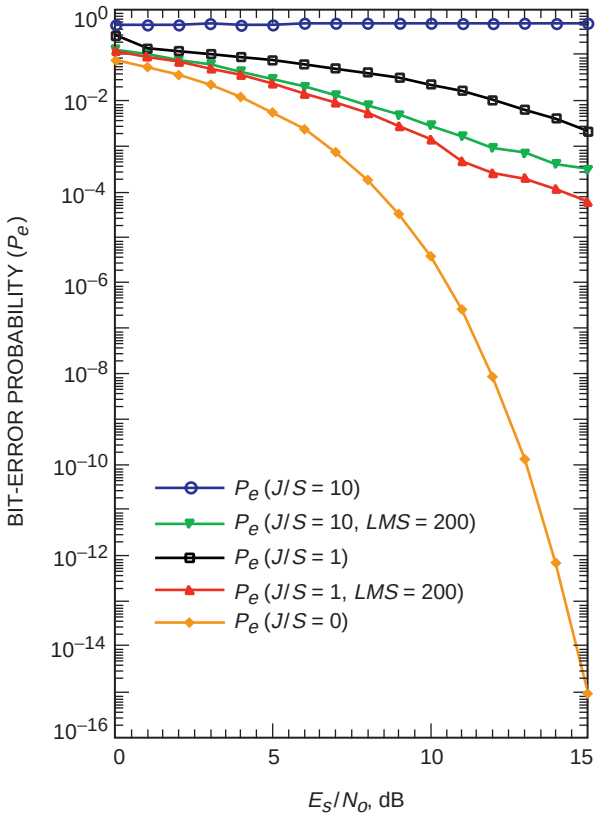

Fig. 4. The bit-error performance of the time-domain RFI-suppression approach as a function of symbol SNR, where Δ = 5 bits, *LMS* = the number of taps, and the normalized frequency offset (to the data rate) between the tone interference and the carrier = 0.5.

The frequency-domain approach was simulated for a similar setup without taking the imperfect knowledge of the interference characteristics into consideration. Figures 5 and 6 show the bit-error performances versus the interference locations and symbol SNRs. These results indicate slightly better performance as compared with those obtained for the time-domain approach, except that the bit-error rate curve of the $J/S = 10$ and DFT = 8192 case has a flat tail (and worse performance) in the high E_s/N_o region. This suggests an irreducible error from the frequency-domain approach when the interference is much stronger than the signal and, therefore, the noise. Under this circumstance, the bit-error performance cannot be improved further since only a fixed portion of the dominant interference is removed by the notch filter. No such irreducible error was found from the time-domain approach since the ALE can separate and cancel the interference from the signal at any given J/S ratio. Furthermore, it is important to know that the performance advantage shown here for the frequency-domain approach may disappear if imperfect knowledge of the tone interference is considered.

V. Conclusion

The RFI problem encountered at Goldstone has many facets. It ranges from externally generated sources, such as nearby military activities or other space communication applications, to some internally generated sources, such as an imperfect antenna configuration or intersite interference. In this article, we narrowed our scope to the in-band RFI suppression. Two CW RFI-suppression techniques, one for time-domain and the other for frequency-domain processing, were presented. The simulated

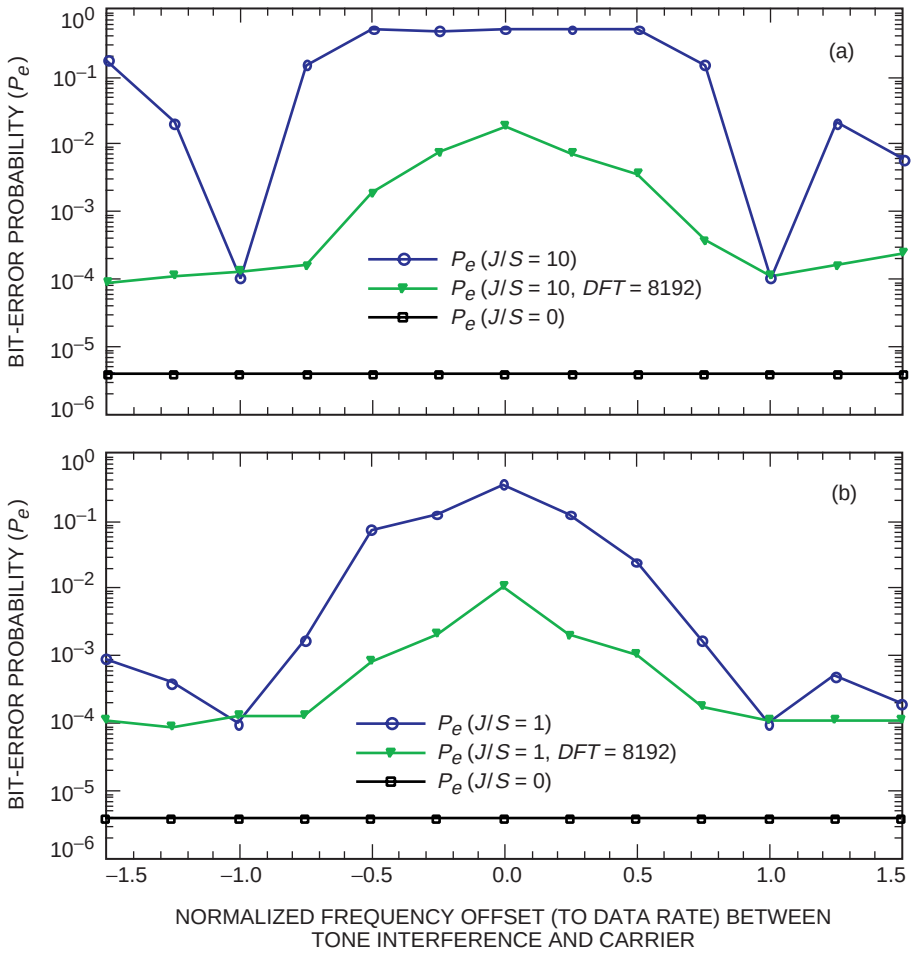

Fig. 5. The bit-error performance of the frequency-domain RFI-suppression approach as a function of tone interference location, where W_n = 20 and DTF = the size of the DFT, when (a) J/S = 10 and (b) J/S = 1.

performances based upon the tracking of a fully suppressed BPSK signal were compared and trade-offs between them discussed.

The performance comparison indicates both approaches are comparable. Under the tested condition, the frequency-domain approach slightly outperforms its counterpart with a priori knowledge of RFI characteristics. However, in real-world applications, it will require intelligent frequency-domain detection and estimation algorithms to adaptively adjust the notch-filter parameters for accurate suppression and respond to the presence or absence of tone interferences. The time-domain approach does not rely on prior knowledge of RFI characteristics. It *learns* the RFI through its adaptive algorithm and can be implemented easily in the existing DSN Block V receiver structure without additional detection/estimation algorithms and dedicated hardware like the CSP.

In conclusion, the time-domain adaptive approach provides the best overall solution for in-band CW RFI suppression for fully suppressed carrier tracking. An improved version of a frequency-domain RFI-mitigation technique with built-in intelligence currently is being developed to deal with a broader range of RFI problems. In the future, detailed RFI tests will be conducted on the DSN Block V receiver to evaluate the effectiveness of all proposed interference-mitigation methods.

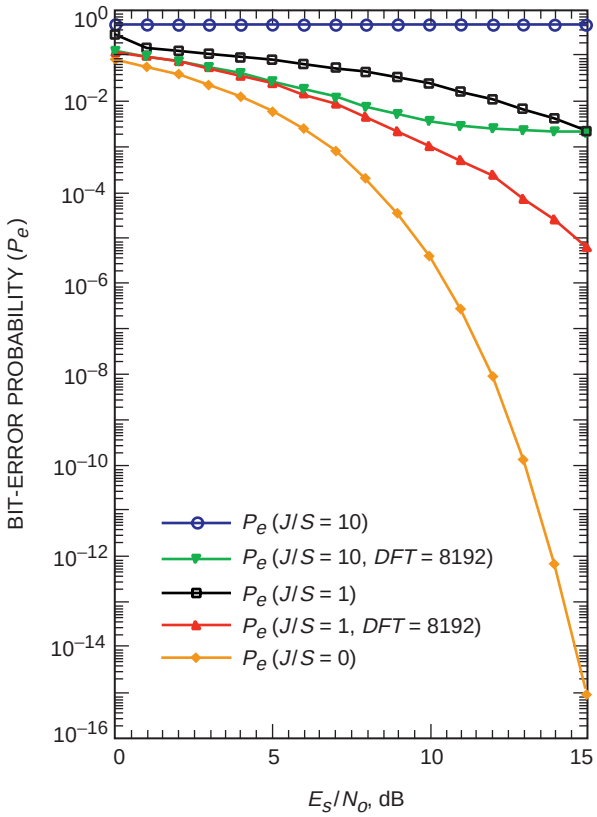

Fig. 6. The bit-error performance of the frequency-domain RFI-suppression approach as a function of symbol SNR, where W_n = 20, DTF = the size of the DFT, and the normalized frequency offset (to the data rate) between the tone interference and the carrier = 0.5.

Acknowledgments

The authors would like to thank Paul Robbins and Miles Sue for providing the RFI incident reports and previous RFI studies performed for the DSN, Helmut Wilck and Mike Grimm for general information on the CSP, Kar-Ming Cheung for his thoughts on issues associated with frequency-domain processing, and Victor Lo for his many valuable comments on various subjects presented in this article.

References

[1] B. Widrow, J. R. Golver, Jr., J. M. McCool, J. Kaunitz, C. S. Williams, R. H. Hearn, J. R. Zeidler, E. Dong, Jr., and R. C. Goodlin, "Adaptive Noise Cancelling: Principles and Applications," *Proceedings of the IEEE*, vol. 63, no. 12, pp. 1692–1716, December 1975.

[2] L. J. Griffiths, "Rapid Measurement of Digital Instantaneous Frequency," *IEEE Transactions on Acoustics, Speech, and Signal Processing*, vol. 23, no. 2, pp. 207–222, April 1975.

[3] D. Morgan and S. Craig, "Real-Time Adaptive Linear Prediction Using the Least Mean Squares Gradient Algorithm," *IEEE Transactions on Acoustics, Speech, and Signal Processing*, vol. 24, no. 6, pp. 494–507, December 1976.

[4] F. Symons, "Narrowband Interference Rejection Using the Complex Linear Prediction Filter," *IEEE Transactions on Acoustics, Speech, and Signal Processing*, vol. 26, no. 1, pp. 94–98, February 1978.

[5] J. R. Zeidler, E. H. Satorius, D. M. Chabries, and H. T. Wexler, "Adaptive Enhancement of Multiple Sinusoids in Uncorrelated Noise," *IEEE Transactions on Acoustics, Speech, and Signal Processing*, vol. 26, no. 3, pp. 240–254, June 1978.

[6] J. Treichler, "Transient and Convergent Behavior of the Adaptive Line Enhancer," *IEEE Transactions on Acoustics, Speech, and Signal Processing*, vol. 27, no. 1, pp. 53–62, February 1979.

[7] C. Anderson, E. H. Satorius, and J. R. Zeidler, "Adaptive Enhancement of Finite Bandwidth Signals in White Gaussian Noise," *IEEE Transactions on Acoustics, Speech, and Signal Processing*, vol. 31, no. 1, pp. 17–28, February 1983.

[8] Y. Yoganandam, V. U. Reddy, and T. Kailath, "Performance Analysis of the Adaptive Line Enhancer for Sinusoidal Signals in Broad-Band Noise," *IEEE Transactions on Acoustics, Speech, and Signal Processing*, vol. 36, no. 11, pp. 1749–1757, November 1988.

[9] L. Milstein, "Interference Rejection Techniques in Spread Spectrum Communications," *Proceedings of the IEEE*, vol. 76, no. 6, pp. 657–671, June 1988.

[10] J. R. Zeidler, "Performance Analysis of LMS Adaptive Prediction Filters," *Proceedings of the IEEE*, vol. 78, no. 12, pp. 1781–1806, December 1990.

[11] G. A. Zimmerman, M. F. Garyantes, M. J. Grimm, and B. Charny, "A 640-MHz 32-Megachannel Real-Time Polyphase-FFT Spectrum Analyzer," *The Telecommunications and Data Acquisition Progress Report 42-107, July–September 1991*, Jet Propulsion Laboratory, Pasadena, California, pp. 132–140, November 15, 1991.

Appendix
The Decimated Inverse DFT

To verify the validity of the decimated inverse DFT described in Section III, we will show that the decimated inverse DFT output, $\hat{y}(n)$, is merely a resampled version of the DFT input, $y(n)$, given in Eq. (7) when there is no spectrum mask applied between the DFT and its inverse. Under this condition, Eq. (10) becomes

$$\begin{aligned} Z(k) =& \frac{1}{D}\sum_{j=1}^{D} Y[k+(j-1)M] \\ =& \frac{1}{D}\sum_{j=1}^{D}\frac{1}{D}\sum_{l=1}^{D} w(l)\sum_{n=1}^{N} x(n-l)e^{-i2\pi[k+(j-1)M]n/N} \\ =& \frac{1}{D}\sum_{l=1}^{D} w(l)\sum_{n=1}^{N} x(n-l)e^{-i2\pi kn/N}\frac{1}{D}\sum_{j=1}^{D} e^{-i2\pi(j-1)nM/N} \\ =& \frac{1}{D}\sum_{l=1}^{D} w(l)\sum_{m=1}^{M} x(mD-l)e^{-i2\pi km/M} \end{aligned} \tag{A-1}$$

since

$$\frac{1}{D}\sum_{j=1}^{D} e^{-i2\pi(j-1)nM/N} = \frac{1}{D}\sum_{j=1}^{D} e^{-i2\pi(j-1)n/D} = \begin{cases} 1, & \text{if } \dfrac{n}{D} \in I \\ 0, & \text{otherwise} \end{cases} \tag{A-2}$$

Substituting Eq. (A-1) into Eq. (11) and comparing the result with Eq. (7), we have

$$\begin{aligned} \hat{y}(n) =& \frac{1}{M}\sum_{k=1}^{M}\frac{1}{D}\sum_{l=1}^{D} w(l)\sum_{m=1}^{M} x(mD-l)e^{-i2\pi k(m-n)/M} \\ =& \frac{1}{D}\sum_{l=1}^{D} w(l)\sum_{m=1}^{M} x(mD-l)\ \delta_{m,n} \\ =& \frac{1}{D}\sum_{l=1}^{D} w(l)x(nD-l) \\ =& y(nD) \end{aligned} \tag{A-3}$$

for $1 \le n \le M$.